A Variational Approach for 3D Motion Estimation of Incompressible PIV Flows

L. Alvarez, C. Castaño, M. García, K. Krissian, L. Mazorra, A. Salgado, and J. Sánchez

Departamento de Informatica y Sistemas
Universidad de Las Palmas de Gran Canaria, Spain
www: http://serdis.dis.ulpgc.es/~lalvarez/ami/index.html

Abstract. Estimation of motion has many applications in fluid analysis. Lots of work has been carried out using Particle Image Velocimetry to design experiments which capture and measure the flow motion using 2D images. Recent technological advances allow capturing 3D PIV image sequences of moving particles. In this context, we propose a new three-dimensional variational (energy-based) technique. Our technique is based on solenoidal projection to take into account the incompressibility of the real flow. It uses the result of standard flow motion estimation techniques like iterative cross-correlation or pyramidal optical flow as an initialization, and improves significantly their accuracies. The performance of the proposed technique is measured and illustrated using numerical simulations.

1 Introduction

"Particle Image Velocimetry (PIV) is a technique which allows one to record images of large parts of flow fields in a variety of applications in gaseous and liquid media and to extract the velocity information out of these images" [1]. The typical setting of a PIV experiment consists in the following components: the flow medium seeded with particles, droplets or bubbles, a double pulsed laser which illuminates the particles twice with a short time difference, a light sheet optics guiding a thin light plane within the flow medium, one or several CCD cameras which capture the two frames exposed by the laser pulses and a timing controller synchronizing the laser and the camera. Once the flow motion has been captured, software tools are needed to evaluate and display the flow motion. The standard techniques work in a planar domain (2D-PIV), permitting estimation of the 2 planar components of the fluid motion (2C-PIV). The third spatial component can also be extracted using stereo techniques, dual-plane PIV or holographic recording (3C-PIV) [2]. The extension of the observation to a volume (3D-PIV) is currently an active area of research. To this end, multicamera configuration or holographic techniques (see [3]) has been proposed.

In this paper, we propose a technique for 3D fluid motion estimation applied to 3D-PIV. The most widely used technique for motion estimation in 2D-PIV is based on local correlation between two rectangular regions of the two images

(see for instance [4]). This technique has a straightforward extension to 3D images. Another approach to motion estimation widely used in optical flow is a variational approach based on an energy minimization where on the one hand, we assume the conservation of the intensity of the displaced objects (in our case the particles) and on the other hand, we assume a certain regularity of the obtained flow. A variational approach was proposed in [5] in the context of 2D PIV. We propose to compare and combine both approaches in order to improve the accuracy of the flow estimation. The proposed method is very general and can be used in many applications of 3D flow estimation.

In the particular case of incompressible fluid motion, we have designed a method to include the incompressibility constraint in the flow estimation.

The paper is organized as follows: in section 2, we briefly describe the motion estimation using local cross-correlation; in section 3, we describe our variational approach and the solenoidal projection; in section 4, we present the numerical experiments followed by the conclusion.

2 Motion estimation using local cross-correlation

Cross-correlation is the most common technique for fluid motion estimation in PIV and is described, for instance, in [1]. We will denote I_1 and I_2 the two images from which we compute the motion $\mathbf{u}$, N the image dimension (in our case $N = 3$) and Ω the domain of definition of the images.

2.1 Basic principle

Having the two volumes I_1 and I_2, for each voxel $\mathbf{v} = (v_x, v_y, v_z)$ of I_1, the method takes a rectangular subvolume $I_{1,\mathbf{v}}$ of I_1 centered on $\mathbf{v}$, and looks for a similar subvolume of I_2 centered on a neighbor $\mathbf{v} + \mathbf{d}$ of $\mathbf{v}$. The similarity measure between two rectangular subvolumes of the same dimensions is based on 2D cross-correlation and is defined as:

$$C_{\mathbf{v}}(I_1, I_2)(\mathbf{d}) = \sum_{\mathbf{y}=(-a,-b,-c)}^{(a,b,c)} I_1(\mathbf{v}+\mathbf{y})\; I_2(\mathbf{v}+\mathbf{d}+\mathbf{y}) \tag{1}$$

The voxel $\mathbf{v}$ is assigned the displacement $\mathbf{d}$ which gives the maximal value of the cross-correlation. Doing this for every voxel in I_1 we obtain a complete vector field $\mathbf{u}$.

2.2 Implementation using Fast Fourier Transform

Because the process of computing the cross-correlation for many subvolumes of I_2 and for each voxel is computationally heavy, the implementation takes advantage of the properties of the Fourier transform to improve the processing

time. The Fourier transform has the property that a correlation in the spatial domain is equivalent to a multiplication in the Fourier domain.

$$C_{\mathbf{v}}(I_1, I_2) = \mathcal{F}^{-1}(\widehat{I_{1,\mathbf{v}}}\ \widehat{I_{2,\mathbf{v}}}^{*}), \tag{2}$$

where $I_{1,\mathbf{v}}$ is a rectangular subvolume of I_1 centered on the voxel $\mathbf{v}$, $\widehat{I_{1,\mathbf{v}}}$ is the Fourier Transform of the subvolume $I_{1,\mathbf{v}}$, the operator * denotes the complex conjugate, and $\mathcal{F}^{-1}$ denotes the inverse Fourier transform. The image $C_{\mathbf{v}}(I_1, I_2)(\mathbf{d})$ gives the result of cross-correlation for all displacements $\mathbf{d}$ and the maximal value is a best estimate of the local displacement. Because of the hypothesis of periodicity introduced by the Fourier Transform, the window is usually chosen four times bigger than the expected displacement. The method is then extended to allow subvoxel accuracy by means of local interpolation of a Gaussian function close to the discrete maximum. When the correlation has been computed for every voxel, some kind of data validation procedure is needed to remove outliers.

Actually, we do not have to compute the correlation for each voxel, we can calculate the flow only for the voxels located on a given lattice. At the end of the process, we extrapolate the results and obtain a dense vector field. This improves not only the speed of the computation, but also in some cases the quality of the results because of the regularization induced by the extrapolation.

The whole process should be applied iteratively a few times using the current result as an initialization for the next iteration. The iterative process can be initialized with a null vector field $\mathbf{u}^0 = 0$, and $\mathbf{u}^{n+1}$ can be estimated at each voxel of the lattice using the displacement with maximal correlation for a window of I_2 displaced by $\mathbf{u}^n$:

$$C_{\mathbf{v}}(I_1, I_2, \mathbf{u}^n) = \mathcal{F}^{-1}(\widehat{I_{1,\mathbf{v}}}\ \widehat{I_{2,\mathbf{v}+\mathbf{u}^n(\mathbf{v})}}^{*}), \tag{3}$$

By doing this, we can improve the accuracy of the fluid motion estimation. It also permits the progressive reduction of the size of the correlation window.

3 Variational Approach

Variational approach to motion estimation are often used for optical flow computation [6–8]. It consists in minimizing an energy as a function of the displacement and that depends on a pair of images I_1 and I_2.

In this section, E will denote the energy functional to minimize. For a given 3D vector field $\mathbf{u} = (u^x, u^y, u^z)^t$, the norm of its gradient $\| \nabla \mathbf{u} \|$ is defined as $\sqrt{\| \nabla u^x \|^2 + \| \nabla u^y \|^2 + \| \nabla u^z \|^2}$, and the Laplacian $\Delta \mathbf{u} = div(\nabla \mathbf{u})$ is defined as $(\Delta u^x, \Delta u^y, \Delta u^z)^t$.

The energy to minimize is expressed as :

$$E(\mathbf{u}) = \underbrace{\int_{\Omega} \left(I_1(\mathbf{x}) - I_2\left(\mathbf{x} + \mathbf{u}(\mathbf{x})\right)\right)^2 d\mathbf{x}}_{data\ term} + \underbrace{\alpha \int_{\Omega} \|\nabla \mathbf{u}(\mathbf{x})\|^2 d\mathbf{x}}_{regularization\ term}, \tag{4}$$

where α is a scalar coefficient that weights the smoothing term. Under the assumption of intensity conservation for each voxel, the first term (*data term*) becomes zero when the first image matches the second one displaced by $\mathbf{u}$: $I_1(\mathbf{x}) = I_2(\mathbf{x} + \mathbf{u}(\mathbf{x}))$. This term tries to find the vector field that best fits the solution. The second term is a *regularization term* which smoothes the vector field. There are a lot of ways to define the regularization term, including, for instance, discontinuities preserving constraints, etc.. In this paper, since we deal with rather smooth flows we use the L_2 norm presented above. Euler-Lagrange equations yield:

$$(I_1(\mathbf{x}) - I_2(\mathbf{x} + \mathbf{u})).\nabla I_2(\mathbf{x} + \mathbf{u}) + \alpha div(\nabla \mathbf{u}) = 0 \tag{5}$$

The coefficient α is normalized to allow invariance under global intensity change. To this purpose, α is multiplied by

$$\alpha = \alpha_0 \left(\epsilon + \sqrt{\frac{1}{|\Omega|} \int_\Omega \|\nabla \mathbf{I_2}(\mathbf{x})\|^2 d\mathbf{x}} \right)^2 \tag{6}$$

with $\epsilon = 0.01$.

3.1 Numerical scheme

We propose to look for the minimum of the energy by solving (5) directly using a fixed point approach. An alternative is to use a gradient descent with either explicit or semi-implicit scheme. We use an iterative method to find the vector field $\mathbf{u}$:

$$\begin{cases} \mathbf{u}^0 & = \mathbf{u_0} \\ \mathbf{u}^{n+1} & = \mathbf{u}^n + \mathbf{h}^{n+1} \end{cases} \tag{7}$$

where we update the vector field $\mathbf{u}$ at each iteration by adding another vector field $\mathbf{h}$ with small displacements. The displacement $\mathbf{h}$ being small, we can use first order Taylor expansions of I_2 and ∇I_2 at $\mathbf{x} + \mathbf{u}^n$ to linearize (5), and we obtain:

$$d\mathbf{g} - \left[\mathbf{g}\mathbf{g}^t - dH'\right] \mathbf{h} + \alpha div(\nabla \mathbf{u}^n + \nabla \mathbf{h}) = 0 \tag{8}$$

denoting:

$$\mathbf{g}(\mathbf{x}) = \nabla I_2(\mathbf{x} + \mathbf{u}^n) \tag{9}$$

$$d(\mathbf{x}) = I_1(\mathbf{x}) - I_2(\mathbf{x} + \mathbf{u}^n) \tag{10}$$

$$H'(\mathbf{x}) = H(I_2)(\mathbf{x} + \mathbf{u}^n). \tag{11}$$

In the last equality, $H(I_2)(\mathbf{x})$ denotes the Hessian matrix of I_2 at the location $\mathbf{x}$. The term in second order spatial derivatives is usually neglected, supposing that the image varies slowly. Then, (8) becomes:

$$d\mathbf{g} + \alpha div(\nabla \mathbf{u}^n) - \mathbf{g}\mathbf{g}^t\mathbf{h} + \alpha div(\nabla \mathbf{h}) = 0 \tag{12}$$

After discretization using finite differences, the operator $div(\nabla \mathbf{h})$ can be divided in two terms $-2N\, I\, \mathbf{h}$ and $S(\mathbf{h})$, where the N is the image dimension and I is the identity matrix. The first term only depends on values of $\mathbf{h}$ at the current position $\mathbf{x}$ and the second term only depends on values of $\mathbf{h}$ at neighbor positions of $\mathbf{x}$: the vector $S(\mathbf{h})$ is written:

$$S(\mathbf{h}) = \begin{pmatrix} \sum_{\mathbf{y} \in N^*(\mathbf{x})} h^x(\mathbf{y}) \\ \sum_{\mathbf{y} \in N^*(\mathbf{x})} h^y(\mathbf{y}) \\ \sum_{\mathbf{y} \in N^*(\mathbf{x})} h^z(\mathbf{y}) \end{pmatrix}, \tag{13}$$

where $N^*(\mathbf{x})$ denotes the direct neighbors of $\mathbf{x}$ (4 in 2D and 6 in 3D), and $\mathbf{h} = (h^x, h^y, h^z)^t$.

Using $\mathbf{h}^{n+1}$ for the current location $\mathbf{x}$ and $\mathbf{h}^n$ for its neighbors, (12) becomes:

$$A\mathbf{h}^{n+1} = b \tag{14}$$

with $A = \mathbf{g}\mathbf{g}^t + \alpha 2N\, I$, and $b = d\mathbf{g} + \alpha div(\nabla \mathbf{u}^n) + S(\mathbf{h}^n)$. The matrix A is real, symmetric and positive definite, so it can be inverted and we can compute for each position $\mathbf{x}$, $\mathbf{h}^{n+1} = A^{-1}b$. To improve the convergence rate, we use a Gauss-Seidel method which updates the displacement $\mathbf{h}^{n+1}$ at position $\mathbf{x}$ using the values of $\mathbf{h}^{n+1}$ already calculated. This scheme is recursive and to avoid privileging the direction of scanning the image, we apply two successive iterations of Gauss-Seidel in reverse directions. Furthermore, we use a pyramidal approach to compute the displacement flow at several scales, using the results from a given scale to initialize to the following higher scale.

4 Refined variational approach

We introduce two modifications to (4) to improve the solution. First, the regularization term is applied to the increment of the displacement vector $\mathbf{h}$ at each iteration instead of the whole vector $\mathbf{u}$. It allows the minimization to be invariant under the solution: if the data term is zero, no smoothing will be applied. This change implies removing the term $\alpha div(\nabla \mathbf{u}^n)$ from (12) while using the same numerical scheme. Second, we replace the solution by its solenoidal projection and re-iterate the minimization to take into account the incompressibility of the flow. This refinement step will use only one scale since it is initialized by the solution of one of the previous methods described in sections 2 or 3. The following paragraph describes the solenoidal projection.

4.1 Solenoidal projection

In our experiments, the fluid flows are *incompressible*. As a consequence, the displacement vector field $\mathbf{u}$ should be divergence-free, i.e. $div(\mathbf{u}) = \frac{\partial u^x}{\partial x} + \frac{\partial u^y}{\partial y} + \frac{\partial u^z}{\partial z} = 0$. One way to fulfill this constraint is to project our estimated motion $\mathbf{u}$

into the space of divergence-free vector field. This new vector field $\mathbf{u}_s$ is called a solenoidal projection of $\mathbf{u}$. It can be expressed as:

$$\mathbf{u}_s = \mathbf{u} - \nabla v, \tag{15}$$

where v is a scalar function of $\Omega \subset \mathbb{R}^3$, defined as a solution to the following *Poisson's equation*:

$$\begin{cases} div(\nabla v) = div(\mathbf{u}) \text{ in } \Omega \\ v = 0 \qquad\quad \text{in } \partial\Omega \end{cases} \tag{16}$$

This equation is solved using Gauss-Seidel technique.

5 Experiments and Results

In this section, we present experiments on synthetic data using both methods (correlation and variational). We used a 3D flow based on realistic flow models to check the performance of the proposed methods. In these experiments, we first apply the standard correlation or variational methods to obtain a good approximation of the flow and then we refine the results with the new variational approach.

5.1 Choice of the parameters

The cross-correlation parameters are the window size in each dimension and the lattice spacing. The window size is approximately set to four times the expected maximal displacement and is the same in each dimension. In the following experiments, we use a lattice spacing of 2 voxels in each dimension, and the final result is interpolated to obtain a dense estimation. The variational approach uses the parameters α and the number of scales for the pyramidal approach. In the following experiments, we set α to 0.5 for both the standard and the refined variational approaches.

5.2 Description of the models

In the first model (Fig. 1, left), we use an incompressible 3D flow model suggested to us by Professor F. Scarano that can be found in [9] (section 3-9.2). It corresponds to the Stokes's solution for an immersed sphere. The flow moves in the horizontal axis direction with a velocity $(U, 0, 0)$, and it avoids the sphere located at the center of the volume. The flow inside the sphere is null.

Having a sphere with radius α and center $(0, 0, 0)$, and a 3D point (x, y, z) at a distance r from the sphere center, the flow outside the sphere follows:

$$\begin{aligned} u &= U\left(1 - \frac{3\alpha}{4r^3}(2x^2 + y^2 + z^2) + \frac{\alpha^3}{4r^5}(2x^2 - y^2 - z^2)\right) \\ v &= U\left(-\frac{3\alpha}{4r^3}xy + \frac{3\alpha^3}{4r^5}xy\right) \\ w &= U\left(-\frac{3\alpha}{4r^3}xz + \frac{3\alpha^3}{4r^5}xz\right) \end{aligned} \tag{17}$$

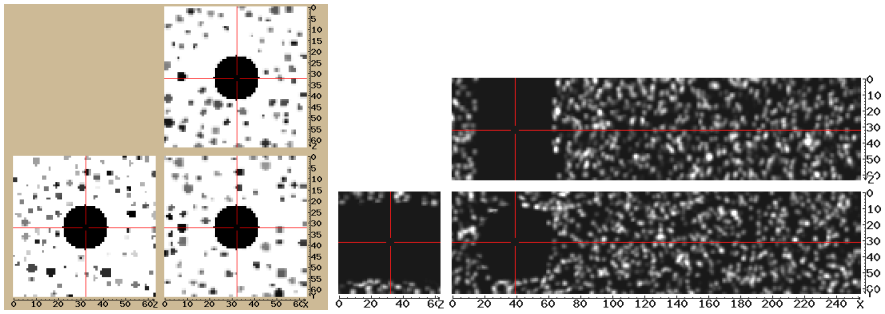

Fig. 1. Left, model 1 (sphere). Right, model 2 (cylinder)

The other model (Fig. 1, right) was provided to us by the Cemagref Rennes, France and it has been obtained using a Large Eddy Simulation of the incompressible Navier-Stokes equations which defines the turbulent motion after a cylinder [10]. It simulates a volume with synthetic particles following the horizontal axis and a cylinder situated on the z-axis obstructing the flow perpendicularly. We use two successive images from this sequence. The original model is a volume of 960 x 960 x 144 voxels but we limit our experiment to a window of 256 x 64 x 64 voxels to reduce the computation time. This window includes part of the cylinder and the turbulence behind it.

5.3 Experiments with model 1 (sphere)

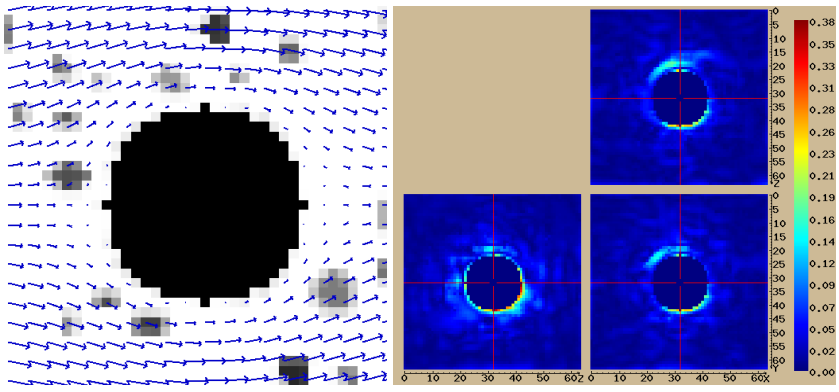

Fig. 2. Left, real flow (with zoom). Right, final error distribution (combined scheme).

Table 1 shows the average error and the standard deviation reached for the cross-correlation and the variational methods before and after the refinement. The error at each voxel is computed as the magnitude of the difference between

	Corr.	Corr.+Ref.	**Var.**	**Var.+Ref.**
av. error	0.029	0.0135	0.03164	0.01702
std. dev.	0.0296	0.0153	0.03033	0.02756

Table 1. Comparison of the two methods for model 1.

the ideal displacement and the estimated one, and is measured in voxel unit. The correlation was applied 11 times with a window size of 8 voxels. The individual variational approach was applied using $\alpha = 0.5$ and 3 scales. The mean error is approximately divided by two after applying the refined variational approach, and the initialization with correlation gives a better result than the initialization with a variational approach. Figure 2 (right) shows the final average error distribution using the cross-correlation followed by the refined variational approach. We can observe that the highest error is located at the sphere boundaries.

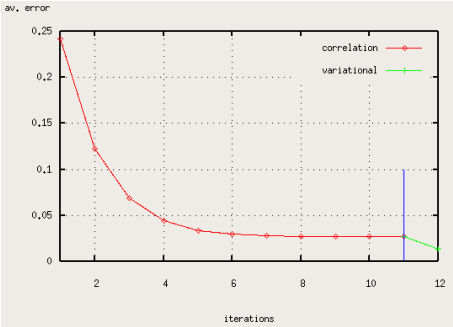

Fig. 3. Left, average error evolution using the combined scheme (11 times cross-correlation + variational).

The left curve in Fig. 3 displays the average error evolution using the combined scheme. First, we apply 11 iterations of correlation technique (we observe that the correlation reaches a stable average error after 11 iterations). Next, we use the output flow provided by the correlation as the input flow of the refined variational technique (curve after iteration 11). We observe a significant improvement in the flow estimation error after using the proposed refined variational method.

5.4 Experiments with model 2 (cylinder)

We ran the same experiments for this model. Table 2 shows the average error and standard deviation reached for the cross-correlation and the variational methods before and after the refinement. The correlation was applied 6 times with a

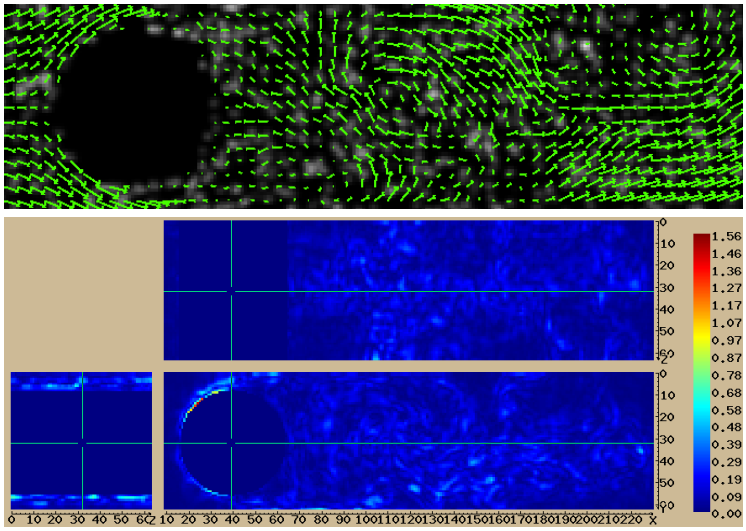

Fig. 4. Top, real flow. Bottom, final error distribution (combined scheme).

	Corr.	Corr.+Ref.	**Var.**	**Var.+Ref.**
av. error	0.1670	0.0651	0.1579	0.0763
std. dev.	0.1375	0.0729	0.1461	0.0891

Table 2. Comparison of the two methods for model 2.

sequence of different window sizes: 16, 16, 8, 8, 4, 4. The variational approach was applied using $\alpha = 0.5$ and 3 scales. Finally, the refined variational method was applied with $\alpha = 0.5$ and one scale. In this experiment, the variational and the correlation correlation methods alone reach similar accuracies, and after the refinement, the cross-correlation reaches a slightly better result. In both cases, the new refined variational approach reduces the mean error by at least half. Figure 4 (bottom) shows the final average error distribution using the combination of the cross-correlation and the refined variational schemes. As in the previous model, the highest error is also located at the obstacle boundaries.

The curve in Fig. 5 displays the average error evolution using the combined scheme of correlation and refined variational approaches. It shows that the correlation reaches a stable average error after 6 iterations and that an additional iteration of the proposed variational approach reduces considerably the mean error.

6 Conclusion

In this paper, we presented an improvement to a standard variational 3D flow estimation technique based on soleinodal projections and a more flexible

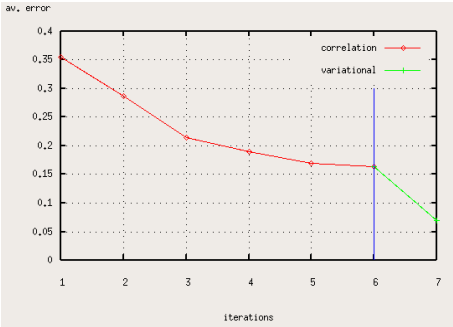

Fig. 5. Average error evolution using the combined scheme (6 times cross-correlation + variational).

smoothing term. The proposed refined variational optical flow technique is initialized by standard techniques like cross-correlation or standard 3D optical flow. We have implemented these techniques and we have shown in the numerical experiments that the proposed technique improves the accuracy of the flow estimation and reduces the mean error by at least half. Slightly better results were obtained by the initialization from cross-correlation, which is probably due to the smoothing term of the standard variational approach that cannot deal with fast variations or discontinuities of the flow close to the obstacle.

Although we focused our attention to 3D fluid flow analysis, the proposed methodology is very general and can be applied to different fields. Correlation based techniques and energy minimization techniques have been developed in the research community in a completely independent way. Each one has its own advantages and limitations but we think that an adequate combination of both can improve the global estimation of the flow. On the other hand, we think that including physical 3D flow constraints, as for instance the incompressibility, to the 3D flow estimation, is a very important issue and allows combining the mathematical models of fluid motion with the experimental data.

In future work, we plan to investigate other regularization terms as proposed in [11, 12], and to compare our current method with approaches which include an incompressibility constraint within the variational formulation [5, 13].

Acknowledgments

This work has been funded by the European Commission under the Specific Targeted Research Project FLUID (contract no. FP6-513663). We acknowledge the Research Institute Cemagref Rennes (France) for providing to us the PIV sequence and Prof. F. Scarano for his valuable comments

References

1. Raffel, M., Willert, C., Kompenhans, J.: Particle Image Velocimetry. A Practical Guide. Springer Verlag (1998)
2. Hinsch, K.D.: Three-dimensional particle velocimetry. Meas. Sci. Tech. **6** (1995) 742–753
3. Royer, H., Stanislas, M.: Stereoscopic and holographic approaches to get the third velocity component in piv. von Karman Institute for Fluid Dynamics, Lecture Series **03** (1996)
4. Scarano, F.: Iterative image deformation methods in piv. Measc. Sci. Technol. **13** (2002) R1–R19
5. Corpetti, T., Heitz, D., Arroyo, G., Mémin, E., Santa-Cruz, A.: Fluid experimental flow estimation based on an optical-flow scheme. Experiments in Fluids **40**(1) (2006) 80–97
6. Horn, B., Schunck, B.: Determining optical flow. MIT Aritificial Intelligence Laboratory (April 1980)
7. Beauchemin, S.S., Barron, J.L.: The computation of optical flow. ACM Computing Surveys **27**(3) (1995) 433–467
8. Barron, J., Fleet, D., Beauchemin, S.: Performance of optical flow techniques. IJCV **12**(1) (1994) 43–77
9. White, F.: Viscous Fluid Flow. McGraw-Hill (2006)
10. Parnaudeau, P., Carlier, J., Heitz, D., Lamballais, E.: Experimental and numerical studies of the flow over a circular cylinder at reynolds number 3900. Physics of Fluids **(submitted)** (2006)
11. Weickert, J., Schnörr, C.: A theoretical framework for convex regularizers in pde-based computation of image motion. International Journal of Computer Vision **45**(3) (2001) 245–264
12. Alvarez, L., Weickert, J., Sánchez, J.: Reliable estimation of dense optical flow fields with large displacements. International Journal of Computer Vision **39**(1) (2000) 41–56
13. Yuan, J., Ruhnau, P., Memin, E., Schnörr, C.: Discrete orthogonal decomposition and variational fluid flow estimation. In Springer, ed.: Lecture Notes in Compute Science (Scale Space 2005). Volume 3459. (2005) 267–278